Consistent changes in the sea ice seasonal cycle in response to global warming

Ian Eisenman *

California Institute of Technology, Pasadena, California, and University of Washington, Seattle, Washington

Tapio Schneider

California Institute of Technology, Pasadena, California

David S. Battisti and Cecilia M. Bitz

University of Washington, Seattle, Washington

ABSTRACT

It has been widely noted that sea ice retreats faster in summer than winter in the Northern Hemisphere, both in observations and in projections from state-of-the-art climate models. Explanations for why the wintertime sea ice cover should be less sensitive to global warming have been proposed. However, in the Southern Hemisphere sea ice retreats fastest in winter in climate model projections. Here we show that the inter-hemispheric differences can be attributed to differences in coastline geometry. After accounting for this geometry, we find that the sea ice changes simulated in both hemispheres in most climate models are consistent with sea ice retreat being fastest in winter in the absence of landmasses. These results demonstrate that despite the widely differing rates of ice retreat among climate model projections, the seasonal structure of the sea ice retreat is robust among the models and uniform in both hemispheres.

1. Introduction

The extent of sea ice covering the ocean in the high northern latitudes varies between about 7 Mm^2 at summer minimum and 15 Mm^2 at winter maximum in today's climate (with 1 $Mm^2 = 10^6$ km^2). During recent decades, Arctic sea ice has been rapidly retreating. The summer minimum of the ice extent has diminished considerably more rapidly than the winter maximum (e.g., Serreze et al. 2007), with an associated increase in the amplitude of the seasonal cycle (Figs. 1A, 2). These changes can also be viewed in the context of first-year and multi-year components of the sea ice cover, a common distinction based on whether or not the ice has survived a summer melt season. In the approximation that all of the ice at summer minimum survives the winter growth season, the winter maximum first-year ice extent is equivalent to the amplitude of the ice extent seasonal cycle (Comiso 2002; Zhang and Walsh 2006). The increased seasonal cycle amplitude of Arctic sea ice extent, or similarly the increase in first-year ice extent, typically features prominently in assessments of recent observed changes in the Arctic sea ice (e.g., Nghiem et al. 2007; Kwok et al. 2009; Perovich et al. 2009).

The observed changes can be compared with global warming projections from state-of-the-art coupled atmosphere-ocean global climate models (GCMs) which were carried out for the Coupled Model Intercomparison Project phase 3 (CMIP3), the results of which were used for the Intergovernmental Panel on Climate Change Fourth Assessment Report (Solomon et al. 2007). GCM projections vary widely in terms of the rate of Arctic sea ice loss (Fig. 3), making it difficult to obtain a reliable estimate for the timescale of future ice retreat (cf. DeWeaver 2007; Boe et al. 2009; Wang and Overland 2009). However, the Arctic sea ice extent seasonal cycle is consistently amplified as the climate warms in most of the GCMs (Fig. 2A,B), which has been identified as one of the most striking features of the Northern Hemisphere sea ice projections (Zhang and Walsh 2006). Hence the GCM projections suggest that whatever is causing Arctic sea ice retreat to be fastest in summer may be expected to continue in the future.

In contrast to the Northern Hemisphere, observations reveal very little long-term change in Southern Hemisphere ice extent, with the trend being toward a slight increase (Fig. 2D,E). Although the positive trend in Southern Hemisphere annual-mean sea ice extent is statistically significant (e.g., Comiso and Nishio 2008), the seasonal differences in the rate are small, and there is no significant change in the seasonal cycle amplitude (see Appendix A). Hence the observed sea ice cover in the Southern Hemisphere has not changed sufficiently to carry implications regarding how the ice extent seasonal cycle amplitude responds to climate

change.

GCM projections, however, show Southern Hemisphere sea ice retreat that is fastest in winter (Fig. 2D,E), opposite to what occurs in the Northern Hemisphere (Fig. 1A). Although this feature can be readily seen in previously published results (Arzel et al. 2006; Solomon et al. 2007, Fig. 10.13), scant discussion of it exists in the literature.

Most previously published physical mechanisms for changes in the sea ice extent seasonal cycle have focused on observed changes in the Arctic. A standard explanation suggests that thin ice reforms in winter wherever air is sufficiently cold but quickly melts during the following summer, causing the summer ice extent to be more sensitive than the winter ice extent to thermodynamic changes induced by increased greenhouse gases (e.g., Meier et al. 2005). Summer minimum ice extent anomalies have also been proposed to be amplified by seasonally-dependent factors including the ice-albedo feedback (Lindsay and Zhang 2005; Perovich et al. 2007), downward longwave radiative flux anomalies (Francis and Hunter 2007), and changes in ocean heat transport driven by the penetration of wind forcing through the sea ice cover (Shimada et al. 2006). However, explanations for the ice retreat being fastest at summer minimum that rely on basic thermodynamic processes and feedbacks are inconsistent with the simulated ice retreat being fastest in winter in the Southern Hemisphere.

Alternatively, natural variability in atmospheric circulation has been proposed as an explanation for a substantial fraction of the observed loss of summer Arctic sea ice extent, with wind-driven ice advection during winter leading to thinner ice that is more easily melted during the following summer (Rigor et al. 2002). This mechanism was supported by observed correlations during the early and mid-1990s, and an associated longer-term reduction in the age of the ice cover was suggested to explain the continued ice retreat thereafter despite the sign of the correlations reversing (Rigor and Wallace 2004). More recently, correlations with another index of atmospheric circulation have been suggested to explain a significant fraction of the observed trend in summer minimum sea ice extent (Ogi et al. 2010). Explanations for the ice retreat being fastest at summer minimum that rely on natural variability in wind forcing, however, are at odds with the Northern Hemisphere sea ice extent seasonal cycle amplitude increasing during the entire 21st century in GCM simulations.

Changes in the sea ice extent seasonal cycle in both hemispheres are summarized schematically in Fig. 1A. Due to the vast differences in the rate of retreat (Fig. 3), we choose a coordinate system here that does not depend on rate. In Fig. 2C,F, the ice extent seasonal cycle amplitude in each hemisphere is plotted versus the annual-mean ice extent. As the annual-mean sea ice edge migrates poleward, the observed and simulated sea ice extent seasonal cycle increases in the Northern Hemisphere (Fig. 2C), whereas the simulated sea ice extent seasonal cycle decreases in the Southern Hemisphere (Fig. 2F). This study examines why the response of the sea ice extent seasonal cycle to global warming is opposite between the two hemispheres.

2. Effect of landmass distribution

Among the wide array of differences in climate between the two hemispheres, we isolate the effect of landmass distribution as the factor likely to have the most pronounced effect on the sea ice cover. In the Northern Hemisphere, there is little land poleward of 75°N, but extensive land south of this rims the Arctic Ocean (Fig. 4A). As a result, the sea ice edge is obstructed by land throughout the year except near the time of summer minimum ice extent. In the Southern Hemisphere, by contrast, the Antarctic continent extends from the pole to about 70°S, but there is little land equatorward of this in the latitudes spanning the Southern Ocean (Fig. 4C). Hence the Southern Hemisphere sea ice edge rarely touches land.

We focus here on the simple obstruction of sea ice by landmasses. The shape of the Northern Hemisphere coastline causes changes in the sea ice edge latitude to have a muted effect on sea ice extent during much of the year (Fig. 4A). In Eisenman (2010), it was proposed that seasonal asymmetries in Arctic sea ice evolution ranging from the shape of the seasonal cycle to the unprecedented loss in September 2007 can be explained in terms of this muting. Here we follow that work's definition of "equivalent extent" as the total land plus ocean surface area poleward of the zonal-mean sea ice edge. The equivalent extent can be approximately visualized by drawing a straight line between the sea ice edge on either side of each landmass and filling in the region poleward of this line with sea ice. This provides a rough approximation of what the sea ice extent might be if all the land were removed.

The equivalent extent is proportional to the sine of the zonal-mean ice edge latitude (Eisenman 2010). In this work we focus on the equivalent extent, rather than on the ice edge latitude, to facilitate comparison with sea ice extent in the Southern Hemisphere, where the sea ice edge evolves in a nearly land-free geography. If the Northern Hemisphere zonal-mean ice edge latitude migrates poleward at a rate that is constant year-round, as is the case during recent decades in observations (Eisenman 2010), the ice extent decreases most rapidly in summer (larger white area between solid and dashed red lines than between blue lines in Fig. 4A). Wintertime changes in the ice edge have a considerably larger effect on equivalent extent than on extent, however, and in this scenario the equivalent extent decreases most rapidly in winter (larger white plus gray area between blue lines than between red lines in Fig. 4A).

We compute the sea ice equivalent extent from the sea

ice extent using a two-step process. First, the latitude characterizing the sea ice edge is approximated by finding the latitude which has an ocean area poleward of it equal to the ice extent (arrows pointing right in Fig. 4B,D). Next, the equivalent extent is computed as the total land plus ocean area poleward of this latitude (arrows pointing left in Fig. 4B,D). This process is carried out for the ice extent time series from observations and GCMs in both hemispheres, with the transfer function being computed separately from the land masks in each GCM (see Appendix B) and in the observed fields (see Appendix A).

3. Results

The observed and simulated changes in sea ice equivalent extent in both hemispheres are plotted in Fig. 5. In the Northern Hemisphere, the summer minimum equivalent extent (Fig. 5A) is similar to the summer minimum extent (Fig. 2A). However, because the wintertime sea ice edge resides at a latitude with a large land fraction, the winter maximum equivalent extent (Fig. 5B) is considerably larger and retreats faster than the winter maximum extent (Fig. 2B). As expected from the cartoon in Fig. 4A, this influence of land is sufficient to cause the seasonal structure of the Northern Hemisphere ice retreat to be reversed: in contrast to the extent, the equivalent extent seasonal cycle amplitude decreases as the ice edge moves poleward in both observations and GCMs (Fig. 5C).

In the Southern Hemisphere, the equivalent extent (Fig. 5D-E) evolves similarly to the extent (Fig. 2D-E) with the addition of a constant equal to the area of the Antarctic continent. Changes in the summer minimum equivalent extent (Fig. 5D) are somewhat enhanced compared with extent changes (Fig. 2D) due to the ice edge touching the Antarctic coastline (Fig. 4C), but the summer minimum equivalent extent still retreats more slowly than the winter maximum equivalent extent. Hence, after accounting for the muting effect of landmasses on sea ice extent changes, the seasonal cycle in equivalent extent decreases in both hemispheres as the ice edge migrates poleward (Fig. 5C,F, Fig. 1B).

The decreasing equivalent extent seasonal cycle amplitude in response to global warming occurs not only in the ensemble mean in both hemispheres (Fig. 5C,F), but also in most individual GCMs. In Fig. 6, the change during 1900–2100 in the equivalent extent seasonal cycle amplitude in each of the 21 GCMs is plotted. The wide spread in horizontal coordinates for either hemisphere is an indication of the inter-model differences in the simulated rate of retreat. The bunching of points near a diagonal line indicates that although the models do not agree on the amount of ice retreat, they do largely agree that the more the annual-mean ice cover diminishes (farther to left in Fig. 6), the smaller the equivalent extent seasonal cycle becomes (farther down in Fig. 6). The agreement among the models on this point is in stark contrast with their projections for the timeline of sea ice changes (Fig. 3). The central message of Fig. 6 is that the sea ice equivalent extent seasonal cycle diminishes in response to global warming in both hemispheres in most models (i.e., most points lie in the lower quadrant of the plot).

4. Discussion

These results allow a comparison between GCM simulations and observations. As has been noted previously (Stroeve et al. 2007), the observed retreat in summer minimum ice extent (red curve in Fig. 3A) is faster than the retreat in most GCM simulations (thin curves in Fig. 3A). Furthermore, annual-mean sea ice extent, which can be visually approximated by the average between summer minima and winter maxima in Fig. 2, diminishes by approximately the same amount in both hemispheres during 1900–2100 in the GCM simulations, in contrast to observed changes during recent decades. The simulated Northern Hemisphere ice extent diminishes slowly during the 20th century and then more rapidly during the 21st century (Fig. 2A,B), whereas the simulated Southern Hemisphere ice extent diminishes at a more constant rate during 1900-2100 (Fig. 2D,E). These differences between GCMs and observations emerge similarly when viewed from the perspective of equivalent extent: the slopes of the red and blue curves during 1979–2009 in Fig. 5A differ by 60%. For the Northern Hemisphere annual-mean equivalent extent versus time (not shown), the slopes differ similarly by 50%. When plotted in a coordinate system that does not depend on the rate of retreat, however, GCMs and observations in the Northern Hemisphere show better agreement, with the slopes of the red and blue curves in Fig. 5C during 1979–2009 (using yearly data) differing by only 3%. Note that the red and blue curves are displaced from each other in Fig. 5C during this time period by 10% in both horizontal and vertical directions.

Discussions comparing sea ice in the two hemispheres typically find more differences than similarities (e.g. Dieckmann and Hellmer 2010). For example, sea ice in the Northern Hemisphere grows primarily through congelation at the ice–ocean interface, whereas in the Southern Hemisphere, where snow accumulation rates are larger, much of the growth occurs at the surface due to flooding under the weight of snow (Petrich and Eicken 2010). In Fig. 2, the Southern Hemisphere sea ice extent seasonal cycle is considerably larger than that in the Northern Hemisphere, with summer and winter extremes both being outside the Northern Hemisphere seasonal range. After accounting for land, however, the sea ice cover seasonal cycles in the two hemispheres become more similar (Fig. 5). The winter maximum equivalent extent is nearly identical in the two

hemispheres in simulations of the 20th century, but the ice edge is farther poleward at summer minimum in the Northern Hemisphere. In Fig. 5C (Northern Hemisphere), the slope of the seasonal cycle amplitude versus annual-mean equivalent extent evolution is 0.5, and in Fig. 5F (Southern Hemisphere) the slope is relatively similar at 0.4. Similarly, in Fig. 6, the distributions for both hemispheres are near each other and both seem to fall near the same diagonal line.

In addition to illuminating the similarities between the sea ice evolutions in the two hemispheres, the equivalent extent may be a useful metric for comparing models because it addresses differences in model coastlines. Total sea ice cover in GCM simulations is typically compared in terms of ice extent (e.g., Zhang and Walsh 2006). There are considerable inter-model differences, however, in the land masks associated with the sea ice concentrations (i.e., fractional sea ice cover) in the CMIP3 archive. Grid boxes with land fractions between 0 and 1 are treated as land in some models but as ocean in others, and ice shelves are treated as land glaciers in some models but as sea ice in others. This causes the ocean area poleward of 70°, for example, to vary by more than 1 Mm^2 among the models, with the inter-model standard deviation being 0.9 Mm^2 in the Northern Hemisphere and 0.4 Mm^2 in the Southern Hemisphere. In other words, two GCMs may simulate Northern Hemisphere sea ice extents that differ by 1 Mm^2 when both are identically simulating a sea ice cover that extends to 70°N. These effects of land mask differences are naturally addressed when instead using sea ice equivalent extent.

In this analysis, we have followed the standard convention of defining ice extent as the area of grid boxes with sea ice concentration of at least 15%. For a given sea ice cover, this definition depends on grid resolution. The sea ice concentration grids for the GCM data in the CMIP3 archive typically have resolutions on the order of 50–100 km, whereas the observed sea ice extent is calculated using a nominally 25 km grid. Sea ice area, defined as the sum of grid box areas scaled by the ice concentration in each box, is independent of resolution, but it is more prone to systematic errors in satellite-derived observations (e.g., Parkinson and Cavalieri 2008). Using sea ice area instead of extent, and hence calculating a sea ice equivalent area, does not qualitatively influence the results presented here (not shown).

Some GCMs become seasonally ice free during the 1900–2100 simulation period. This edge effect could in principle lead to winter sea ice cover retreating faster than summer ice cover after the latter reaches 0 (cf. Fig. 1). In Fig. 7A, the results of Fig. 6 are repeated for each hemisphere excluding all models that simulate less than 0.1 Mm^2 sea ice extent in that hemisphere at any point during 1900-2100. Comparison of the two figures demonstrates that this effect does not qualitatively affect the results presented in Fig. 6.

The physical mechanism causing sea ice equivalent extent to decrease more rapidly in winter than summer is expected to differ from previously proposed mechanisms, since the latter were aimed at explaining why Northern Hemisphere ice retreat is fastest in summer. Several hints regarding the cause of the changes in the sea ice seasonal cycle can be gleaned from the GCM simulations. First, all but one of the GCMs include horizontal ice motion and rheology. The model INM CM3.0 (#12 in Fig. 6), however, simulates the sea ice as motionless. That this lies near the middle of the distribution in both hemispheres is evidence that horizontal ice motion is not a primary factor. Second, there is considerably more simulated snowfall on the sea ice in the Southern Hemisphere than in the Northern Hemisphere (Solomon et al. 2007, Fig. 8.5), which is typically associated with the difference in land fraction immediately equatorward of the sea ice cover. Additionally, ocean circulation is considerably different between the two hemispheres. That the equivalent extent seasonal cycle changes similarly in both hemispheres is evidence that snow cover and ocean circulation are not dominant factors. Third, five CMIP3 GCMs reported sea ice changes in equilibrium simulations of CO_2 doubling that did not include a dynamic ocean (see Appendix B). The results of these simulations are plotted in Fig. 7B. Similar to Fig. 6, most of the points lie in the lower quadrant, which demonstrates that the equivalent extent seasonal cycle amplitude decreases in response to global warming in both hemispheres in most of these GCMs even in the absence of changes in ocean heat flux convergence. Taken together, these results implicate the interaction between sea ice and atmospheric processes as a likely source of the changes in the sea ice seasonal cycle.

In summary, Northern Hemisphere sea ice extent diminishes faster in summer than winter in observations and GCM projections. Southern Hemisphere sea ice extent, by contrast, diminishes fastest in winter. The results presented here show that after accounting for landmasses that rim the Arctic Ocean, the changes in the sea ice cover in both hemispheres are consistent with ice retreat being fastest in winter in the absence of land. This diminished sea ice cover seasonal cycle in response to warming is robust among the range of GCMs and uniform in both hemispheres.

Acknowledgments.

IE was supported by a Prize Postdoctoral Fellowship through the Caltech Division of Geological and Planetary Sciences and a NOAA Climate and Global Change Postdoctoral Fellowship administered by the University Corporation for Atmospheric Research. We thank the modeling groups and the Program for Climate Model Diagnosis and Intercomparison for making available the CMIP3 multi-

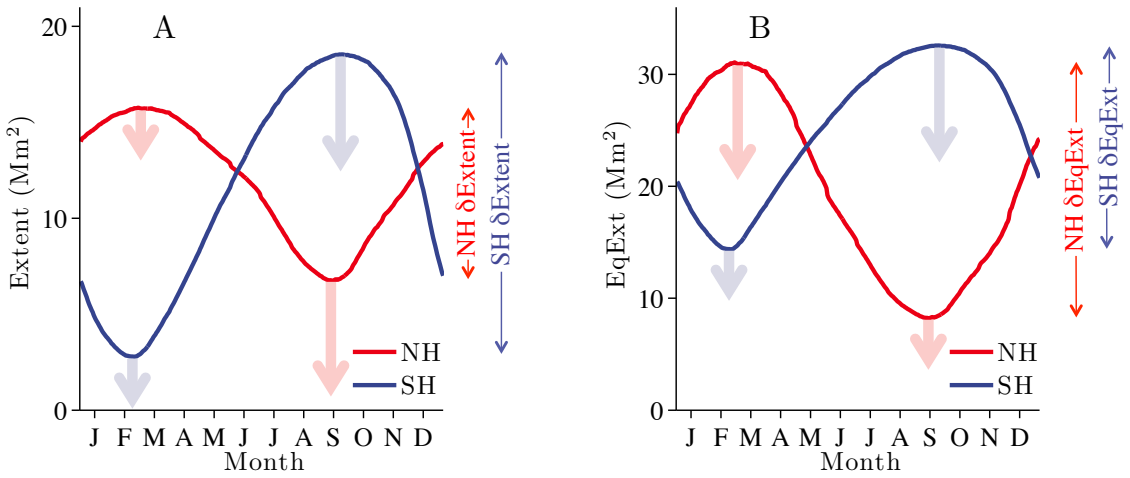

FIG. 1. Schematic illustrating the difference between the rate of change at summer minimum and winter maximum in both hemispheres. (A) Sea ice extent (as plotted in Fig. 2). (B) Sea ice equivalent extent (as plotted in Fig. 5), which represents a rough approximation of what the ice extent would be in the absence of landmasses. Thin double-headed arrows on the right in panel A identify the amplitude of the seasonal cycle. Thick arrows below the curves indicate the rate of change at summer minimum and winter maximum. Curves are drawn from satellite-derived daily sea ice extent (Cavalieri et al. 1996), with equivalent extent computed as described in the text. The lengths of the thick arrows are exaggerated to highlight the points discussed here.

model dataset.

APPENDIX A

Satellite-derived Observations

Data processing

Monthly-mean ice extent observations in both hemispheres are derived from passive microwave satellite measurements during Jan 1979–Dec 2009 (Fetterer et al. 2002). Months with missing values (in both hemispheres, Dec 1987 and Jan 1988) are filled with linear interpolation between the same month in the previous year and following year. We use the NSIDC land mask associated with sea ice concentrations from Nimbus-7 SMMR and DMSP SSM/I satellite measurements to compute sea ice equivalent extent.

Statistical significance in Southern Hemisphere

The annual-mean sea ice extent in the Southern Hemisphere increases during 1979-2009 with a linear trend of 0.15 Mm^2/decade, or 1.2%/decade when scaled by the 1979-2000 mean. This trend is significant above the 99.7% confidence interval (i.e., white noise would produce a trend this far from zero less than 0.3% of the time). The trend in the ice extent seasonal cycle amplitude as a function of time, however, is not distinguishable from zero at even the 68% confidence interval. The same applies for the trend in the yearly ice extent seasonal cycle amplitude versus yearly annual-mean ice extent, as well as the trend in the 5–year averages of these quantities (red points in Fig. 2F).

APPENDIX B

Climate Models

Coupled Atmosphere–Ocean Simulations

We include in this analysis 21 of the 24 coupled atmosphere–ocean GCMs that participated in CMIP3, excluding two (GISS EH and NCAR PCM) that have not reported sea ice concentration fields to the CMIP3 archive for the simulations we analyze and one (LASG FGOALS-g1.0) that has a known bias toward vast overestimation of sea ice extent and is typically excluded from sea ice analyses (e.g., Zhang and Walsh 2006). For each model, ice extent during 1900-2100 is calculated as the total area of grid boxes with at least 15% sea ice concentration in the "Climate of the 20th Century" simulation, and ice extent during 2000-2100 is calculated in the same way from the "SRES A1B" simulation. When multiple ensemble members are available, we consider only the first member.

Land masks for computing equivalent extent in each GCM were obtained using one of several techniques. For many of the GCMs, land grid boxes were reported as missing values in the sea ice concentration field. For GCMs

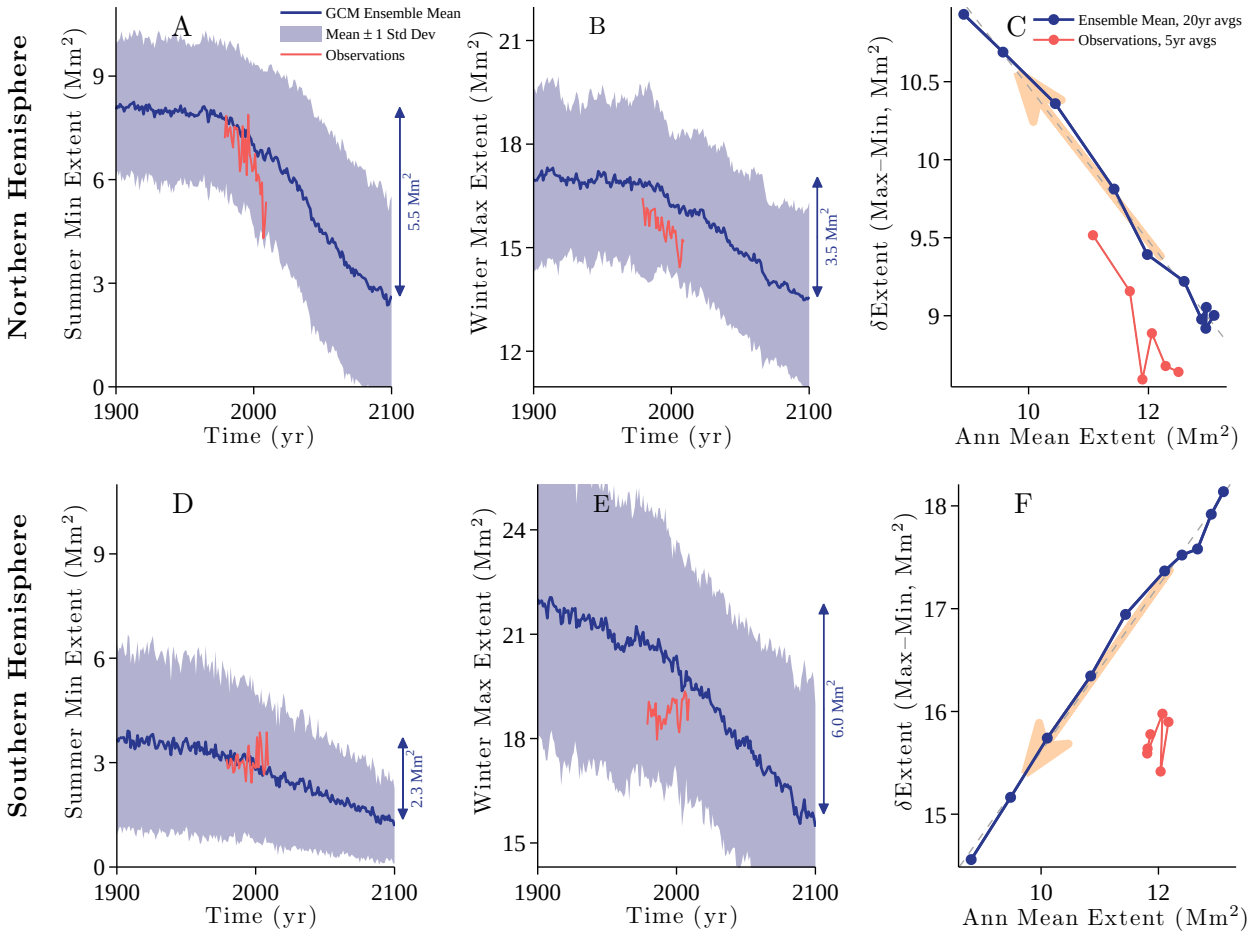

FIG. 2. Observed and simulated changes in sea ice extent in both hemispheres. The Northern Hemisphere (A) summer minimum and (B) winter maximum ice extent are plotted based on monthly-mean satellite-derived observations (see Appendix A) and simulations from 21 coupled atmosphere–ocean GCMs (see Appendix B). (C) The seasonal cycle amplitude is plotted as a function of the annual-mean ice extent, with 20–year averages taken of the ensemble mean and 5–year averages taken for the observations, which span only 31 years. (D)-(F) Same as (A)-(C) but for the Southern Hemisphere. The simulated change in the Southern Hemisphere ice extent seasonal cycle amplitude (panel F) is opposite to the Northern Hemisphere (panel C). Observed Southern Hemisphere changes show very little structure in this context (panel F). Vertical scales in panels A, B, D, and E are all identical.

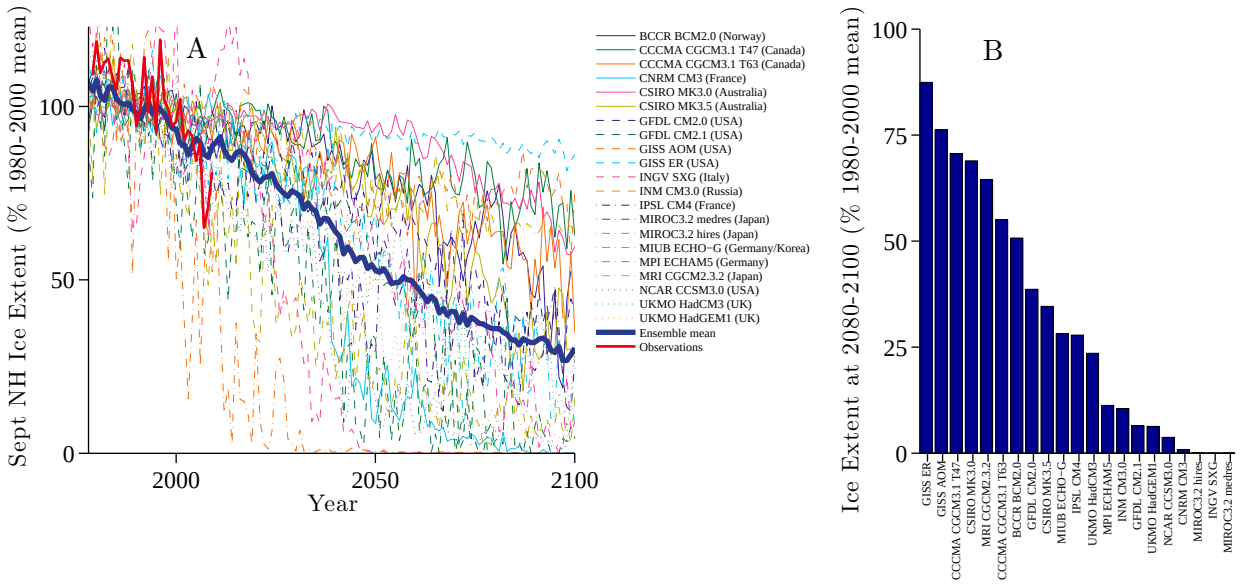

FIG. 3. Differences among the GCM projections of the rate of Arctic sea ice loss. (A) Timeline toward seasonally ice-free Arctic Ocean conditions indicated by September Northern Hemisphere sea ice extent during the 21st century scaled by the 1980–2000 mean September value for each model. (B) Sea ice retreat during the entire 21st century (September extent at 2080–2100 scaled by September extent at 1980–2000) in each GCM. In the ensemble mean, 32% of the September sea ice cover remains at the end of the century, but projections vary widely among the GCMs from a model that retains more than 85% of the ice to 4 models retaining less than 1%.

that instead reported land grid boxes as having zero sea concentration, either missing values in the sea surface temperature field reported by the ocean component or nonzero values in the land area fraction reported by the atmosphere component (which always had values of either 0 or 1 for these models) were used, depending on whether the sea ice component in each GCM shared its grid with the ocean or the atmosphere.

Atmosphere–Ocean Simulations

We also consider atmosphere–only simulations above a slab ocean with specified ocean heat flux convergence (i.e., "ocean q-flux"). Sea ice concentration for these simulations was reported to the CMIP3 archive by 5 of the 24 GCMs. To assess the change in the sea ice cover in response to CO_2 doubling, we calculate the sea ice extent time series from the "slab ocean control" simulation and the "2xCO2 equilibrium" simulation, and then we compute the mean ice extent seasonal cycle during the final 20 years of each simulation. Note that HadGEM1 becomes seasonally ice free in both hemispheres in the "2xCO2 equilibrium" simulation but none of the other 4 GCMs simulate less than 0.1 Mm^2 ice extent in either hemisphere.

Land masks in the slab ocean simulations are identical to the coupled simulations from the same GCM with the exception of HadGEM1, in which the sea ice concentration was reported on the atmosphere grid in the former but on the ocean grid in the latter.

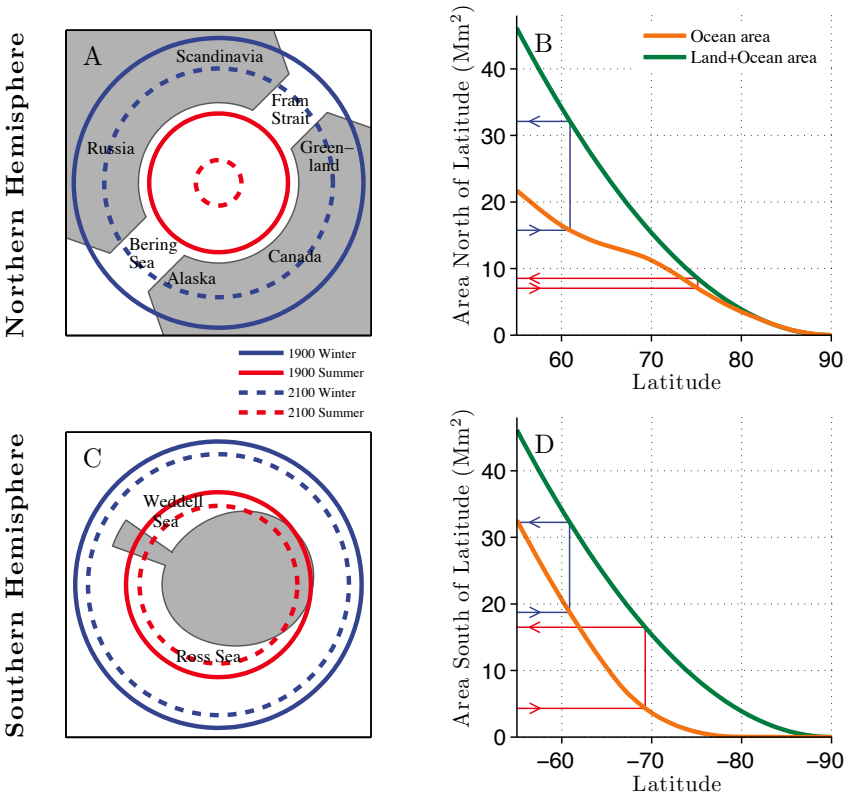

FIG. 4. Cartoon of landmass distributions in both hemispheres and schematic illustrating the calculation of sea ice equivalent extent from extent. (A) Cartoon of Northern Hemisphere geography, with gray indicating land and white indicating ocean. The latitude of the sea ice edge associated with summer minimum (red) and winter maximum (blue) ice cover at the beginning (solid) and end (dash) of the simulated period is included based on the ensemble mean ice edge latitude during 1900–1920 and 2080–2100. The total white area enclosed within a given ice edge line indicates the ice extent, and the total white plus gray area enclosed within the line indicates the equivalent extent. (B) Mapping function used to calculate the sea ice equivalent extent from the extent. The blue line indicates the mapping of a typical Northern Hemisphere winter maximum ice extent to equivalent extent. Beginning with the ice extent (lower intersect of blue line with vertical axis), the latitude with area poleward of it equal to the extent is computed (intersect between blue and orange lines). Next, the total land plus ocean area poleward of this latitude is identified as the equivalent extent (upper intersect of blue and orange lines). The red line indicates the mapping for a typical summer minimum ice extent, illustrating that the difference between equivalent extent and extent is considerably larger at winter maximum than at summer minimum. (C)-(D) Same as (A)-(B) but for Southern Hemisphere. Here the difference between extent and equivalent extent is similar at winter maximum (blue line) and at summer minimum (red line).

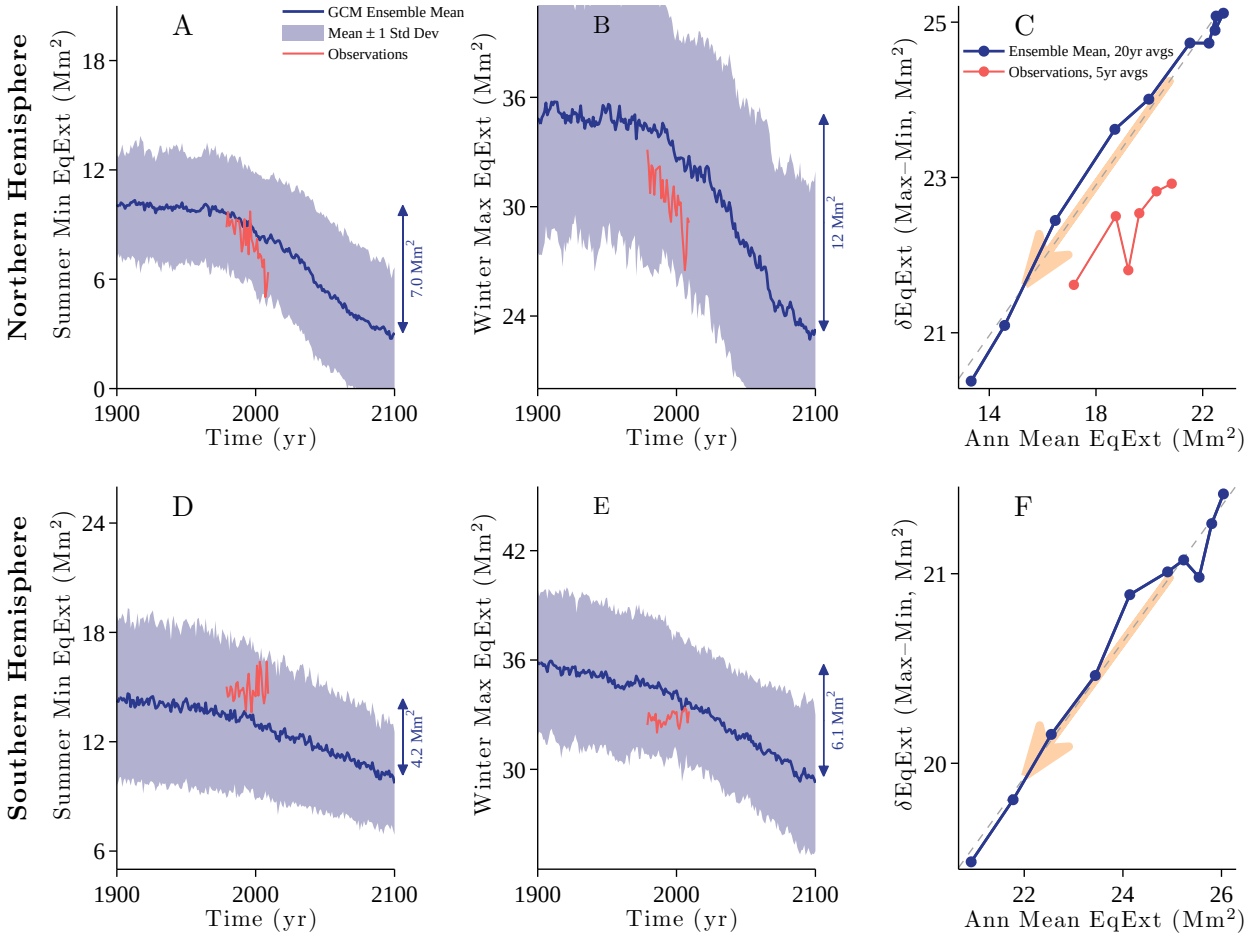

FIG. 5. Observed and simulated changes in sea ice equivalent extent in both hemispheres. Panels are as in Fig. 2. In contrast to the extent, the equivalent extent seasonal cycle responds to global warming similarly in both hemispheres (panels C,F). Note that observed equivalent extent changes in the Southern Hemisphere cluster near the point (26, 18) in panel F and are not included in the plotted vertical range.

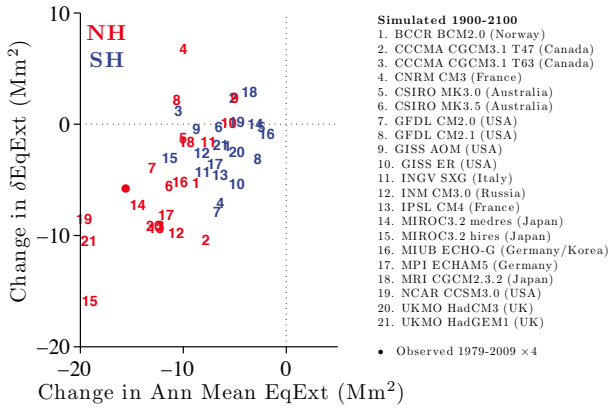

FIG. 6. Robustness among models. The change in the equivalent extent seasonal cycle amplitude during 1900–2100 in each GCM is plotted versus the change in annual-mean equivalent extent for the Northern Hemisphere (red) and the Southern Hemisphere (blue). Vertical and horizontal coordinates here are equivalent to the vertical and horizontal displacements in Fig. 5C,F evaluated separately for each model. That all points lie to the left of the origin indicates that all GCMs simulate a loss of annual-mean ice cover in both hemispheres in response to increased greenhouse gases. More striking is the feature that most points lie below the origin, indicating that most GCMs simulate a reduction in the sea ice equivalent extent seasonal cycle in both hemispheres. Observed Northern Hemisphere changes during the shorter 31–year period are included in the figure after being scaled by a factor of 4. Changes during 1900–2100 are computed by multiplying by 2 the difference between the temporal mean during the first and last 100 years; changes during 1979–2009 are computed similarly using the first and last 15 years.

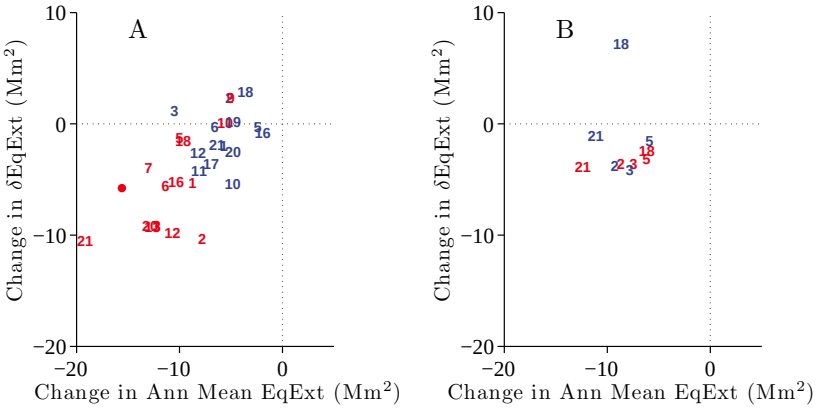

FIG. 7. Influence of edge effects and ocean dynamics on robustness among models. (A) As in Fig. 6, except that for each hemisphere, models with ice extent less than 0.1 Mm^2 at any time during 1900–2100 are excluded. (B) As in Fig. 6, but considering atmosphere–only equilibrium climate sensitivity simulations rather than coupled atmosphere–ocean transient simulations (see Appendix B). Here the differences between the climate under doubled CO_2 and the control simulation are plotted.

REFERENCES

Arzel, O., T. Fichefet, and H. Goosse, 2006: Sea ice evolution over the 20th and 21st centuries as simulated by current AOGCMs. *Ocean Model.*, **12 (3-4)**, 401–415.

Boe, J. L., A. Hall, and X. Qu, 2009: September sea-ice cover in the Arctic Ocean projected to vanish by 2100. *Nature Geosci.*, **2 (5)**, 341–343.

Cavalieri, D., C. Parkinson, P. Gloerson, and H. Zwally, 1996: Sea ice concentrations from Nimbus-7 SMMR and DMSP SSM/I passive microwave data, 1978–2007. *Natl. Snow and Ice Data Cent., Boulder, Colo.*, (Updated 2008.) http://nsidc.org/data/nsidc-0051.html.

Comiso, J. C., 2002: A rapidly declining perennial sea ice cover in the arctic. *Geophys. Res. Lett.*, **29 (20)**, 1956, doi:10.1029/2002GL015650.

Comiso, J. C. and F. Nishio, 2008: Trends in the sea ice cover using enhanced and compatible AMSR-E, SSM/I, and SMMR data. *J. Geophys. Res.*, **113 (C2)**, C02S07, doi:10.1029/2007JC004257.

DeWeaver, E., 2007: Uncertainty in climate model projections of Arctic sea ice decline: an evaluation relevant to polar bears. Tech. rep., U.S. Geological Survey, 40 pp. http://www.usgs.gov/newsroom/special/polar_bears.

Dieckmann, G. S. and H. H. Hellmer, 2010: The importance of sea ice: An overview. *Sea Ice*, Wiley-Blackwell, 2d ed., 1–22.

Eisenman, I., 2010: Geographic muting of changes in the Arctic sea ice cover. *Geophys. Res. Lett.*, **37**, L16 501.

Fetterer, F., K. Knowles, W. Meier, and M. Savoie, 2002: Sea ice index. *Natl. Snow and Ice Data Cent., Boulder, Colo.*, (Updated 2010.) http://nsidc.org/data/seaice_index/archives/.

Francis, J. A. and E. Hunter, 2007: Drivers of declining sea ice in the Arctic winter: A tale of two seas. *Geophys. Res. Lett.*, **34 (17)**, L17 503.

Kwok, R., G. F. Cunningham, M. Wensnahan, I. Rigor, H. J. Zwally, and D. Yi, 2009: Thinning and volume loss of the Arctic Ocean sea ice cover: 2003-2008. *J. Geophys. Res.*, **114**, C07 005.

Lindsay, R. W. and J. Zhang, 2005: The thinning of Arctic sea ice, 1988-2003: Have we passed a tipping point? *J. Climate*, **18 (22)**, 4879–4894.

Meier, W., J. Stroeve, F. Fetterer, and K. Knowles, 2005: Reductions in Arctic sea ice cover no longer limited to summer. *Eos Trans. AGU*, **86 (36)**, 326.

Nghiem, S. V., I. G. Rigor, D. K. Perovich, P. Clemente-Colón, J. W. Weatherly, and G. Neumann, 2007: Rapid reduction of Arctic perennial sea ice. *Geophys. Res. Lett.*, **34 (19)**, L19 504.

Ogi, M., K. Yamazaki, and J. M. Wallace, 2010: Influence of winter and summer surface wind anomalies on summer Arctic sea ice extent. *Geophys. Res. Lett.*, **37**, L07 701, doi:10.1029/2009GL042356.

Parkinson, C. L. and D. J. Cavalieri, 2008: Arctic sea ice variability and trends, 1979-2006. *J. Geophys. Res.*, **113 (C7)**, C07 003, doi:10.1029/2007JC004558.

Perovich, D., R. Kowk, W. Meier, S. Nghiem, and J. Richter-Menge, 2009: Sea ice cover. *Arctic Report Card 2009*, http://www.arctic.noaa.gov/reportcard.

Perovich, D. K., B. Light, H. Eicken, K. F. Jones, K. Runciman, and S. V. Nghiem, 2007: Increasing solar heating of the Arctic Ocean and adjacent seas, 1979-2005: Attribution and role in the ice-albedo feedback. *Geophys. Res. Lett.*, **34 (19)**, L19 505, doi:10.1029/2007GL031480.

Petrich, C. and H. Eicken, 2010: Growth, structure and properties of sea ice. *Sea Ice*, Wiley-Blackwell, 2d ed., 23–77.

Rigor, I. G. and J. M. Wallace, 2004: Variations in the age of Arctic sea-ice and summer sea-ice extent. *Geophys. Res. Lett.*, **31 (9)**, L09 401.

Rigor, I. G., J. M. Wallace, and R. L. Colony, 2002: Response of sea ice to the Arctic oscillation. *J. Climate*, **15 (18)**, 2648–2663.

Serreze, M. C., M. M. Holland, and J. Stroeve, 2007: Perspectives on the Arctic's shrinking sea-ice cover. *Science*, **315 (5818)**, 1533–1536.

Shimada, K., T. Kamoshida, M. Itoh, S. Nishino, E. Carmack, F. McLaughlin, S. Zimmermann, and A. Proshutinsky, 2006: Pacific Ocean inflow: Influence on catastrophic reduction of sea ice cover in the Arctic ocean. *Geophys. Res. Lett.*, **33 (8)**, L08 605, doi:10.1029/2005GL025624.

Solomon, S., D. Qin, M. Manning, Z. Chen, M. Marquis, K. A. M. Tignor, and H. Miller, (Eds.) , 2007: *Climate change 2007: The Physical Science Basis. Contribution of Working Group I to the Fourth Assessment Report of the Intergovernmental Panel on Climate Change*. Cambridge University Press, Cambridge, UK, 996 pp.

Stroeve, J., M. M. Holland, W. Meier, T. Scambos, and M. Serreze, 2007: Arctic sea ice decline: Faster than forecast. *Geophys. Res. Lett.*, **34 (9)**, L09 501, doi:10.1029/2007GL029703.

Wang, M. Y. and J. E. Overland, 2009: A sea ice free summer Arctic within 30 years? *Geophys. Res. Lett.*, **36**, L07 502.

Zhang, X. D. and J. E. Walsh, 2006: Toward a seasonally ice-covered Arctic Ocean: Scenarios from the IPCC AR4 model simulations. *J. Climate*, **19 (9)**, 1730–1747.